



Research on Out-of-Plane Shear Mechanical Properties of Damaged Composite T-joints

Xuanjia Zhang¹, Heyuan Huang^{1,2(✉)}, and Dong Wang¹

¹ School of Aeronautics, Northwestern Polytechnical University, Xi'an 710072, China
huangheyuan@nwpu.edu.cn

² Aircraft Strength Research Institute, Aviation Industries of China, Xi'an 710072, China

Abstract. Composite materials have been widely used in the aviation field because of their light weight, large modulus and high strength. In this paper, the interface mechanical properties of composite T-joints under shear load are tested through experiments, which concluded that the ultimate load of the structure with defects is reduced from 29.01 kN to 27.40 kN and its bearing capacity is reduced by 5.5%. Then, based on the Cohesive Zone Model (CZM), a progressive damage model is established for damage failure analysis. The results show that the damage under shear load mainly extends from both sides to the center. When there is a prefabricated defect in the interface layer, the initial damage occurs near the defect and spreads to both ends of the load direction.

Keywords: Composite materials · T-joints · Out-of-plane shear · Experimental test

1 Introduction

In order to reduce the structural weight while meeting the load-bearing requirements, composite T-stiffened panels have developed from secondary load-bearing structures such as flaperons to main load-bearing structures including fuselage and wings. However, the adhesive joint of the composite T-stiffened panels usually is the weakest part in the structure. At present, some researches have been conducted at home and abroad for the T-shaped structure of Composite stiffened panels. Luo and Xiong et al. [1] compared the failure load of RTM (resin transfer moulding) composite T-joints under tension and bending loads and deduced the failure mechanism, concluding that the resin matrix at the triangular filling area of the joint and the web of the fascia first appears to debond. As the load increases, the web is completely separated from the bottom skin. Bai et al. [2] used progressive damage models (PDMs) to further analyze the initial damage and damage evolution of T-joints under tensile load. Li et al. [3] established the finite element model of the micro-carbon nanotube reinforced composite T-joint by using the cohesion zone unit and studied the damage initiation, evolution and final failure process of the T-joint interface layer. Wu et al. [4] established a finite element model of the composite T-joint structure under tensile loading based on the Tsai-Wu damage criterion and the

cohesive zone model, simulating and analyzing the damage mechanism, load carrying capacity, and interlaminar damage behavior.

There are currently some researches on the joints of T-stiffened panels in aircraft structures, but they generally focus on the bearing capacity and failure mechanism of the joints under tensile and compressive loads. There are few studies on the bearing capacity and failure mechanism of the structure under shear load. In this paper, the joint interface bearing capacity and damage evolution process of T-joint defective and non-defective structures under shear load are studied. Firstly, the load-bearing capacity of T1100/QY8911 composite T-joint was tested through experiments. Then a progressive damage model was established based on the cohesive zone model (CZM) to achieve effective prediction of the strength and damage evolution of the T-joint.

2 Experiment

T-joint is composed of skin and web. The skin layer is $[45/0/-45/90/0/90/-45/0/45/0]$ s and the layers of two ribs about web respectively are $[45/-45/0/45/45/-45/0/45/-45/90/45/-45]$, $[-45/45/90/-45/45/0/-45/45/45/0/-45/45]$. The defect is realized by inserting an iron foil with a radius of 15 mm between the skin and the webs. The size of specimens and the position of the strain gauge are shown in Fig. 1(a). The test form is shown in Fig. 1(b). Four specimens were tested and the test results are shown in Table 1.

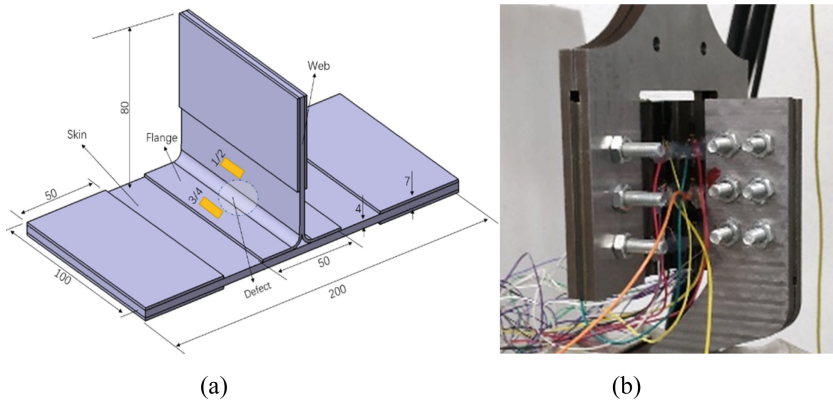


Fig. 1. T-joint test piece and test form: (a) test size of T-joint specimen; (b) loading device

Table 1. Test results

Item	Non-defective shear	Defective shear
Ultimate load (kN)	29.01	27.40

3 Numerical Simulation Method

3.1 CZM Constitutive Model

In this paper, the cohesive zone model was used to simulate the interface damage of T-joint. The stiffness degradation of the bonding interface material properties was carried out according to the bilinear constitutive model, so as to implement the simulation of the interface layer damage initiation and damage evolution [5–7].

The secondary nominal stress criterion [8–10] in the traction-separation rule is used to define the initial damage. In predicting the delamination expansion, when the inter-layer energy release rate is greater than the critical energy release rate, the damage expands and the B-K [11, 12] criterion is used here. Three-dimensional Hashin [13, 14] failure criterion is adopted for the failure of T-type panels.

3.2 Finite Element Model

A three-dimensional finite element model of the T-joint is established based on ABAQUS (see Fig. 2). A layer of cohesive units is set between the flange and the skin of the T-shaped structure. When the unit fails completely, it is deleted to actualize the initiation and expansion of damage about the interface material. Cohesive contact is used between the triangular filling area and the fillet area of the ribs. The unit parameters of the cohesive area are shown in Table 2. Table 3 shows the mechanical properties of the T1100/QY8911 unidirectional composite material.

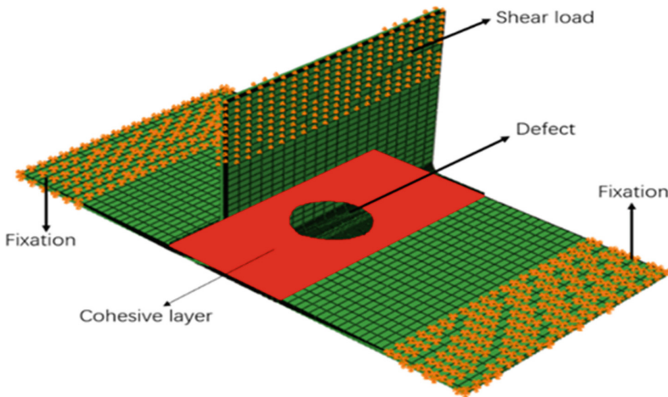


Fig. 2. Finite element model

Table 2. Mechanical properties of cohesive element [15, 16]

Item	Value
G_{Ic} (kJ/m ²)	0.111
G_{IIc} (kJ/m ²)	0.501
t_n^0 (MPa)	13.474
t_s^0 (MPa)	6.999
t_t^0 (MPa)	6.999

Note: t_n^0 is the normal tensile strength of the cohesive unit; t_s^0, t_t^0 is the two shear strengths perpendicular to the crack surface. G_{Ic} is critical fracture energy release rates of I mode and G_{IIc} is critical fracture energy release rates of II mode

Table 3. Mechanical property parameters of T1100/QY8911 materials

Property	Value
Longitudinal tensile strength	2733 MPa
Longitudinal compressive strength	1470 MPa
Transverse tensile strength	62 MPa
Transverse compressive strength	216 MPa
In-plane shear strength	95 MPa

4 Results and Discussion

4.1 Model Validation

In order to verify the validity of the model in this paper, the results of experimental and numerical methods are compared. For T-shear, the ultimate load obtained by the non-defective structure experiment is 29.01 kN and the ultimate load calculated by the finite element method is 30.190 kN, which has a calculation error is 3.91%. The ultimate load obtained by the defective structure experiment is 27.40 kN and the ultimate load calculated by the finite element method is 29.795 kN, which has a calculation error of 8.04%. It can be seen the test results and the numerical results have small errors and high accuracy. The results of specimens show that the load increases linearly with the increase of displacement in the OA section, which is a linear elastic stage. Table 4 records the moment when the sound of structural failure was heard during the experiment. When loaded to 24 KN, the sound of the first layered failure can be heard. Combined with the curve in Fig. 3(a), the AB section is not completely straight, indicating that the specimen has been damaged and destroyed, but it still has the load-bearing capacity until the specimen is destroyed. Due to the existence of defects, the structural rigidity

is reduced and load of structure containing defects has a slight increase after decreasing abruptly (see Fig. 3(b)).

Table 4. Structural failure load values at various stages

	The first destructive sound	The second destruction sound
Load(kN)	24	29

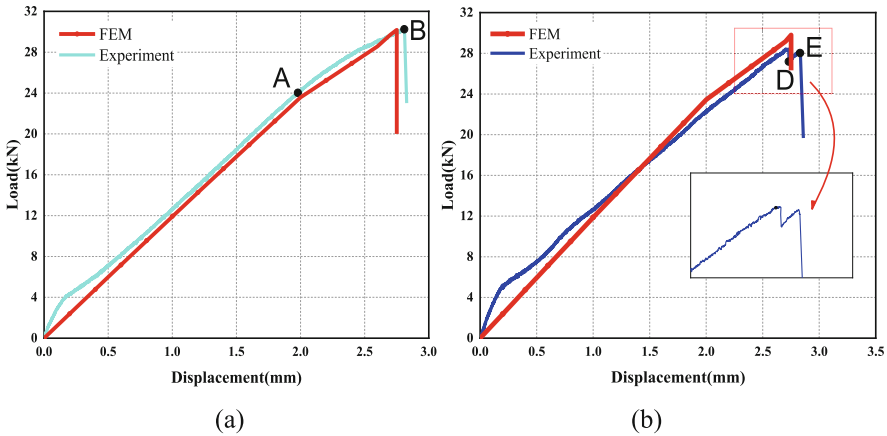


Fig. 3. Comparison of simulation and test results: (a) Intact structure; (b) Defective structure

By testing the strain of structures with intact and defected adhesive interfaces, it is found that there is almost no difference in the variation of strains between the two structures. Therefore, Fig. 4 shows the variation of the strain of the structure with defect as the load increases. During the test of strain, measuring point 1 and measuring point 2 are symmetrical and measuring point 3 and measuring point 4 are symmetrical. It can be seen from these measuring points that the strain of the L-type flange is significantly smaller than the strain of the web. When the shear force is transmitted to the L-shaped bottom surface glued to the skin, it is transformed into the entire bottom surface to bear the load. The cross section of the web is smaller and the strength is greater, so the strain is also greater. When the load reaches 23.8 k N, the sound of slight adhesive layer cracking and fiber breakage can be heard, and the strain changes from point A to point B. When the load reaches 29.01 k N (Point C in Fig. 4), the bonding interface between the T-joint web and the skin is completely debonded, The strain drops abruptly and the structure completely fails, which corresponds to points B and E of the finite element curve in Fig. 3(a) and Fig. 3(b). The test results are highly consistent with the simulation results.

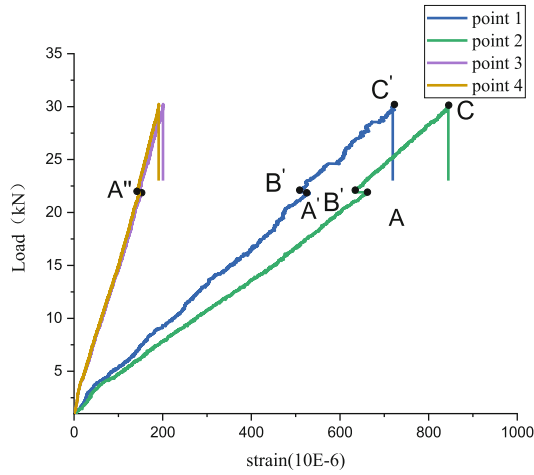


Fig. 4. Load-strain curve

Combined with the finite element stress-strain analysis, it is concluded that the stress is not equally distributed in the interface layer due to that the local force transmission of the web and the existence of the triangular filler that changes the property of the load transmission. The maximum stress of the intact structure is located on both sides of the center of the interface layer, and the maximum strain is located at both ends of the interface layer (see Fig. 5(a) and (b)). The existence of circular defects reduces the

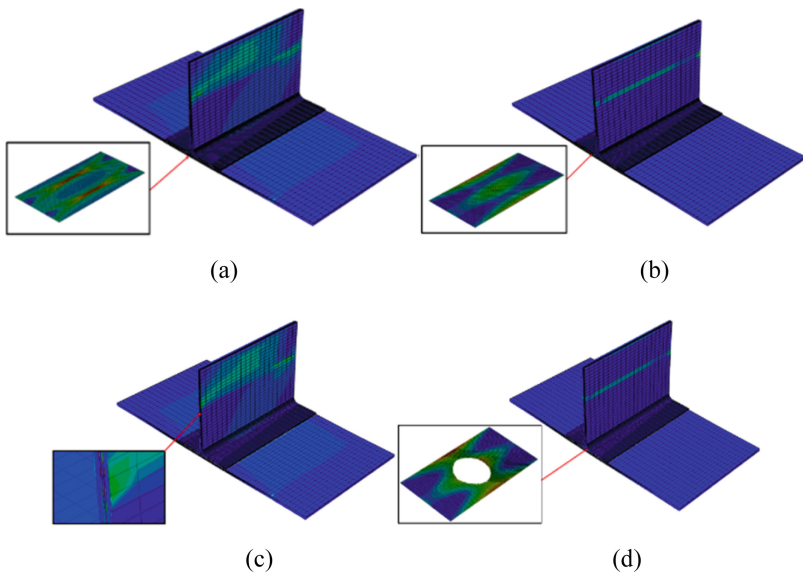


Fig. 5. Structure without damage: (a) stress distribution; (b) strain distribution; structure with damage: (c) stress distribution; (d) strain distribution

bearing capacity of the interface, which changes the property of the load during the force transmission process, making the stress of the interface layer smaller than the clamping section. In addition, the defects reduce the rigidity of the glued joints so that the maximum strain appears around and on both sides of the circular damage position of the interface layer (Fig. 5(c) and (d)).

4.2 Structural Damage Failure Analysis

It can be seen from the experimental results (see Fig. 6) that the T-type web is completely separated from the skin. The non-defective T-joint shear appears irregular fiber breakage at the connection interface and cracks in the glue layer, large area delamination, and a small amount of fiber is pulled out (see Fig. 6(a)). The defective T-joint expands regularly along both sides of the damaged area and the fiber fracture is relatively neat. The fracture of the fiber along the shear direction shows that the fiber has a certain hindering effect on the shear failure of the interface adhesive. Combining the analysis results of the damage model in Fig. 6(a) and (b), there are two paths for damage extension to the T-joint intact structure: one is extending from the two sides perpendicular of loading direction (lateral) to the middle; The other is to extend from the center of the joint along the load direction (longitudinal) to both ends. The defect-containing T-joint extends from the circular defective location in a direction parallel to the load. From Fig. 7(a) to Fig. 7(c), it can be concluded that, due to the high stress level near the loading end, both intact and defected T-joint appears large matrix compression damage and delamination near the loading end, which is consistent with the experimental results.

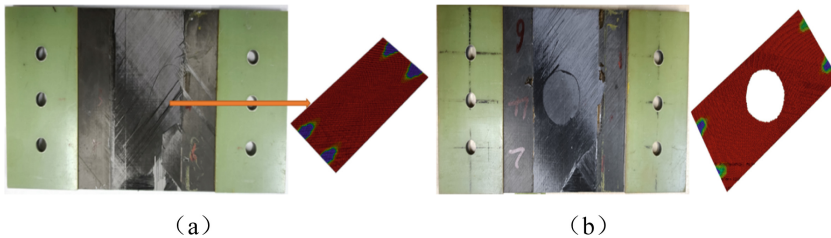


Fig. 6. Interface debonding test results: (a) Debonding appearance without defect side bending; (b) Debonding appearance with defect side bending

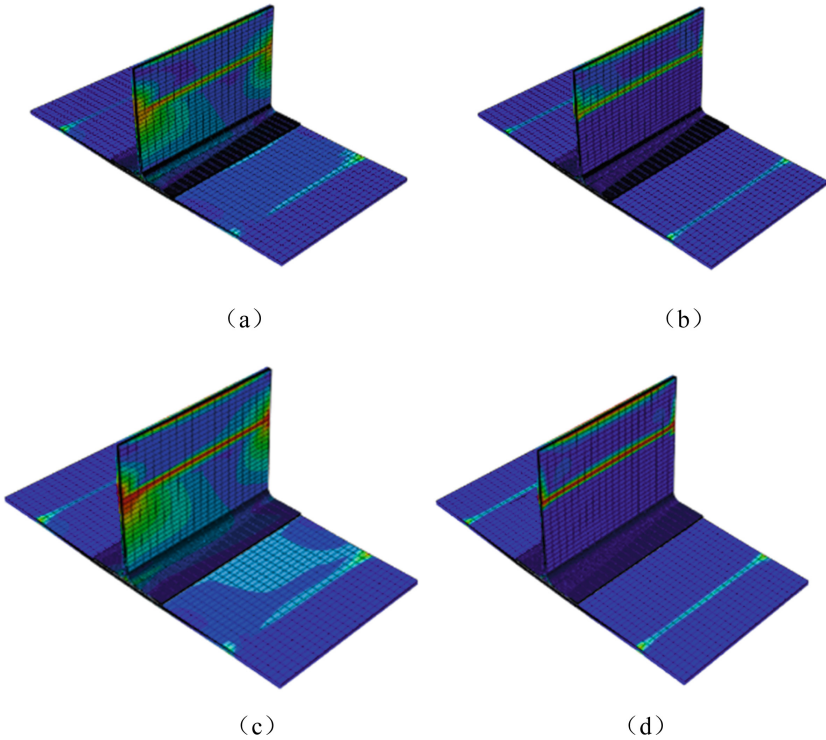


Fig. 7. No defects: (a) matrix failure; (b) laminate delamination failure; including defects: (c) matrix failure; (d) laminate delamination failure

5 Conclusions

This paper conducts a comprehensive study on the bonding interface of composite T-joint under shear load. The mechanical properties of T1100/QY8911 composite T-joints with defect and no defect under shear load were tested through experiments. A finite element numerical method based on the CZM constitutive model was established, which revealed the load-bearing characteristics of the structure and the law of damage evolution. The conclusions are summarized as follow.

- (1) For the T-joint with a defect area of 28% of the bonding surface, the ultimate load of the structure containing defects has been reduced from 29.01 kN to 27.40 kN and its load-bearing capacity has dropped by 5.5%.
- (2) Under the shear load, the damage expands from both sides to the center; when structure contains defects, the damage expands from both sides to the center while also extending longitudinally from the defect position. Due to the high stress level near the loading end, the T-joint appears larger matrix compression damage and laminate delamination near the loading end.

Acknowledgements. This study was supported by the Innovation Capability Support Plan of Shaanxi Province (No. 2020KJXX-067), the Key Research and Development Plan of Shaanxi Province (2020GY-183).

References

1. Luo, C., Xiong, J.: Static pull and push bending properties of RTM-made TWF composite tee-joints. *Chin. J. Aeronaut.* **25**(2), 198–207 (2012)
2. Bai, J.B., Dong, C.H., Xiong, J.J., et al.: Progressive damage behaviour of RTM-made composite T-joint under tensile loading. *Compos. B Eng.* **160**, 488–497 (2019)
3. Li, Q., Zhu, M., Tao, G.Q., et al.: Experimental and numerical investigation of T-joints with multiwalled carbon nanotubes. *Polym. Compos.* **42**(4), 2135–2146 (2021)
4. Wu, H., Xiao, J., Xing, S., et al.: Numerical and experimental investigation into failure of T700/bismaleimide composite T-joints under tensile loading. *Compos. Struct.* **130**, 63–74 (2015)
5. Cui, H., Li, Y., Liu, Y., et al.: Numerical simulation of composites joints failure based on cohesive zone model. *Fuhe Cailiao Xuebao (Acta Materiae Compositae Sinica)* **27**(2), 161–168 (2010)
6. Goyal, V.K., Johnson, E.R., Davila, C.G.: Irreversible constitutive law for modeling the delamination process using interfacial surface discontinuities. *Compos. Struct.* **65**(3–4), 289–305 (2004)
7. Turon, A., Camanho, P.P., Costa, J., et al.: A damage model for the simulation of delamination in advanced composites under variable-mode loading. *Mech. Mater.* **38**(11), 1072–1089 (2006)
8. Wagner, W., Balzani, C.: Simulation of delamination in stringer stiffened fiber-reinforced composite shells. *Comput. Struct.* **86**(9), 930–939 (2008)
9. Alfano, G.: On the influence of the shape of the interface law on the application of cohesive-zone models. *Compos. Sci. Technol.* **66**(6), 723–730 (2006)
10. Brewer, J.C., Lagace, P.A.: Quadratic stress criterion for initiation of delamination. *J. Comp. Mater.* **22**(12), 1141–1155 (1988)
11. Wiggensraad, J.F.M., Aoki, R., Gädke, M., et al.: Damage propagation in composite structural elements—analysis and experiments on structures. *Compos. Struct.* **36**(3–4), 173–186 (1996)
12. Benzeggagh, M.L., Kenane, M.: Measurement of mixed-mode delamination fracture toughness of unidirectional glass/epoxy composites with mixed-mode bending apparatus. *Compos. Sci. Technol.* **56**(4), 439–449 (1996)
13. Hashin Z. Failure criteria for unidirectional fiber composites (1980).
14. Hashin, Z.: Analysis of composite materials—a survey (1983)
15. Cheng, X., Xiong, J., Peng, B., et al.: Mechanical properties of RTM-made composite cross-joints. *Chin. J. Aeronaut.* **22**(2), 211–217 (2009)
16. Murakami, S.: Continuum Damage Mechanics of Composite Materials. In: Murakami, S. (ed.) *Continuum Damage Mechanics*, pp. 277–303. Springer Netherlands, Dordrecht (2012). https://doi.org/10.1007/978-94-007-2666-6_10